fied as ΔP^n in the last equality. By comparing Eqs. (A1) with the exact expression (13), we find that

$$|\Delta P^n \Delta U^n| = \mathcal{O}(\Delta t^2) \tag{A2}$$

Now, we rearrange the right side of Eq. (14) as

$$\Delta V_1^n - (\Delta V_1^n)_{ex} = \Delta P^n \Delta U^n + (\Delta P^n - \Delta P^{n-1}) U^n \tag{A3}$$

In view of Eq. (A2) together with $|\Delta P^n - \Delta P^{n-1}| = \mathcal{O}(\Delta t^2)$, we infer that $\epsilon = \mathcal{O}(\Delta t^2)$.

Acknowledgments

I wish to thank Richard Beam for pointing out a flaw in the original manuscript. Correspondence with him has been invaluable for me to understand the so-called Beam and Warming's implicit scheme, which is de facto standard in computational work. Also, thanks to Miguel Visbal for introducing me to Beam and Warming's scheme and for discussing consequences of the decomposition reported herein.

References

[1]Beam, R. M., and Warming, R. F., "An Implicit Factored Scheme for the Compressible Navier-Stokes Equations," *AIAA Journal,* Vol. 16, 1978, pp. 393-402.

[2]Beam, R. M., and Warming, R. F., "An Implicit Finite-Difference Algorithm for Hyperbolic Systems in Conservative-Law Form," *Journal of Computational Physics,* Vol. 22, 1976, pp. 87-110.

[3]Agnew, R. P., *Differential Equations,* McGraw-Hill, New York, 1942, p. 288.

Formation of Shocks Within Axisymmetric Nozzles

E. Loth,* J. Baum,† and R. Löhner‡
Naval Research Laboratory, Washington, D.C. 20375

I. Introduction

THE formation of shocks within axisymmetric supersonic nozzles has received considerable attention in the past, both experimentally and computationally. The presence of undesirable oblique shocks can significantly alter the downstream flowfield, reduce the thrust efficiency, and affect both the external acoustic signature and base pressure. The experimental study by Back and Cuffel[1] described formation of an oblique shock just downstream of the throat for a tested nozzle geometry and documented centerline Mach number distribution based on pitot stagnation pressures. Measured radial pitot stagnation pressure distributions at the nozzle exit and two locations downstream were obtained for a second nozzle exiting into vacuum ambient conditions with a significantly different nozzle contour.[2] Typical past predictions of internal and external nozzle flow include approximate methods,[3] the method of characteristics,[4] and finite difference schemes.[5]

Recently, unstructured adaptive grids in conjunction with conservative nonlinear shock-capturing schemes have been used to yield fine-grid resolution near high flow gradients. The ability of these codes to capture and predict sharp shocks and contact discontinuities has been demonstrated and validated.[6,7] The newly developed axisymmetric finite element method-flux corrected transport (FEM-FCT) scheme[8,9] is used here to investigate the flow and types of shock formation for various nozzle configurations.

II. Numerical Method

The Euler equations for axisymmetric compressible flow of an ideal gas can be discretized to form a conservative scheme.[7] The two-step second-order Taylor-Galerkin algorithm has been used for the computation of inviscid and viscous flows for the Cartesian[7,8] and axisymmetric[6] coordinate systems. In the first predictor step, the conserved quantitites are assumed piecewise constant, and for the second corrector step, they are assumed piecewise linear. Spatial discretization is performed via the Galerkin weighted residual method, with interpolation conducted separately on the conserved quantities and the radial distance. This leads to a higher accuracy in the r direction[9] and allows a closed-form derivation of the weighted residual statements.

Two types of artificial viscosity are added to the high-order scheme just mentioned (which is essentially fourth-order phase accurate). The first is mass diffusion, which is added to yield a monotonic low-order scheme. The low-order term contribution is combined with the high-order term contribution near admissible discontinuities through the FEM-FCT[7] formulation to prevent the formation of overshoots or undershoots in the conserved quantities. To maintain strict conservation, this limiting is carried out on the element level.[7] The FCT scheme has been shown to be highly robust and accurate for several fluid dynamics problems using both finite difference (see Ref. 10) and finite element schemes.[6-8,11] In addition, the modified Lapidus artificial viscosity, which proved successful for Cartesian coordinate systems, is extended to the axisymmetric case.[6] A Lapidus coefficient of 2 was used, which maintained flux conservation but did extend contact discontinuities for over typically four cells.

Adaptive remeshing was employed to optimize the distribution of grid points by refining areas of high density gradients and coarsening areas of low density gradients. The remeshing allowed a balanced (and efficient) distribution of truncation errors by controlling the relative size of local computational cells. Such remeshing may reduce storage and CPU requirements by 10-100 times in advection-dominated flows as compared to an overall fine grid.[8] The remeshing was accomplished automatically with the advancing front grid generator and typically requires three to four grid adaptations for a steady-state flow solution.

The subsonic inflow boundary conditions employed three characteristic conditions to update boundary values. Along the nozzle wall, tangent flow was imposed such that all fluxes normal to the wall were eliminated. Finally, outflow boundary conditions were set to be free (i.e., no correction on predicted values) for supersonic outflow, which assumes a sufficiently low enough backpressure (which is consistent with the experimental operating conditions). Further boundary condition discussion may be found in Löhner et al.[6] All computations were performed on a Cray X-MP 2/4 using local time stepping and typically took less than half an hour of Cray CPU time to converge.

III. Results and Discussion

Various internal and external axisymmetric nozzle flowfields were predicted using the FEM-FCT scheme. Figure 1a

Received April 2, 1990; presented as Paper 90-1655 at the AIAA 21st Fluid Dynamics, Plasmadynamics, and Lasers Conference, Seattle, WA, June 18-20, 1990; revision received Feb. 22, 1991; accepted for publication Feb. 22, 1991.

*Aerospace Engineer, Laboratory for Computational Physics and Fluid Dynamics; currently Assistant Professor, Department of Aeronautical and Astronautical Engineering, University of Illinois at Urbana-Champaign, Urbana, IL 61801. Member AIAA.

†Senior Research Scientist, Laboratory for Computational Physics and Fluid Dynamics; currently Senior Research Scientist, Science Applications International Corporation, McLean, VA 22102. Member AIAA.

‡Staff Scientist, Berkeley Research Associates, Springfield, VA; currently Research Professor, Civil, Mechanical, and Environmental Engineering, School of Engineering and Applied Science, George Washington University, Washington, DC 20052. Member AIAA.

shows Mach number contours for the nozzle used by Back and Cuffel.[1] The subsonic inlet flow accelerates from left to right and reaches sonic speeds near the throat and continues to accelerate along the centerline until it reaches a maximum Mach number of 3.6. Compression waves are initiated along the wall surface just downstream from the throat and propagate toward the axis of symmetry. These waves coalesce to form an oblique shock that is further strengthened as it approaches the axis, due to the axisymmetric reduction in cross-sectional flow area. This oblique shock formation has been previously documented experimentally[1] and computationally.[4,5] The cause stems from the flow expanding rapidly just downstream of the throat due to the throat's small wall radius of curvature. As the flow enters the conical section, the high angular momentum must be reduced to meet the tangential wall boundary conditions. This is accomplished by a compression wave, which occurs near the discontinuous change in wall curvature.

Figure 1b shows the finite element computational mesh for the nozzle flow. The adaptive mesh has refined regions of high density gradients, such as the shock wave, whereas the regions in which relatively weak density changes occur were resolved only to the preset maximum element size. Figure 1c shows a comparison of the predicted and measured Mach number distribution along the nozzle centerline. The experimental data clearly show the presence of an oblique shock at a relative axial location x, at a distance of seven times the throat radius r_t ($x/r_t = 7$), downstream of the inlet. Previous predictions along with the present analysis show reasonably good agreement upstream of the shock. However, the present analysis yields improved agreement of both the shock strength and subsequent downstream flow.

Figures 2 show flowfield predictions for the second nozzle investigated. Mach number and low-level pressure contours are shown in Figs 2a and 2b. These indicate the formation of two sets of compression waves near the wall, which eventually coalesce to form two oblique shocks. This particular nozzle contour (fitted with a spline) employed a conical (constant slope) section between a circular-arc throat and a parabolic-arc aft section. The two slope changes resulted in the formation of compression waves; the two resulting shocks reduced the thrust efficiency by 7% as compared to an ideal shockless nozzle. In addition, the parabolic-arc section produced an almost continuous set of compression waves originating from the nozzle wall. Because of effects of axisymmetry, these compression waves became curved and resulted in a strong radial pressure gradient at the exit plane, with the highest gradient near the wall. This stands in marked contrast to the typical exit flow gradients noted for the first nozzle (Fig. 1a). Figure 2c shows a comparison of experimental[2] and predicted radial distributions at the exit plane of pitot pressure normalized by the inlet stagnation pressure. At the exit plane, the radial nonuniformity of Mach number is noted both experimentally and computationally.

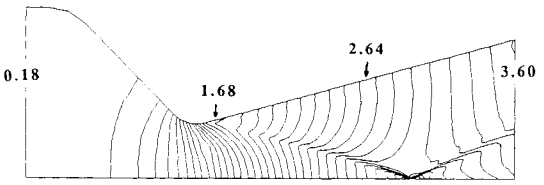

a) Mach number contours of flowfield

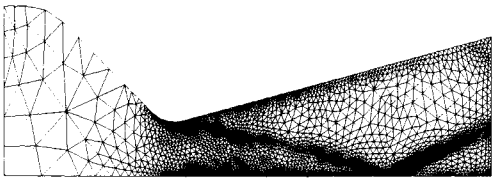

b) Finite element adaptive unstructured mesh, 4990 elements

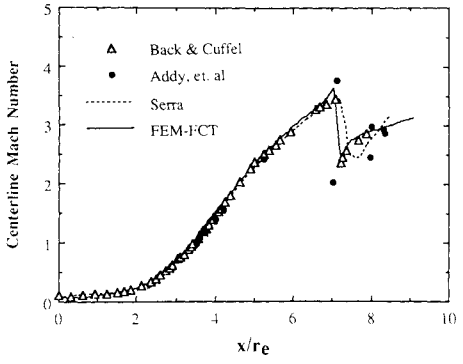

c) Mach number distribution along centerline

Fig. 1 Predictions of Back and Cuffel[1] nozzle flow.

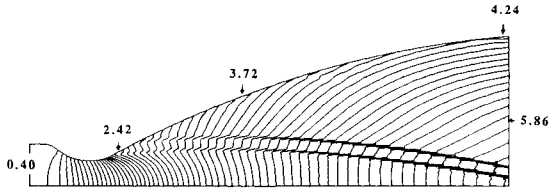

a) Mach number contours of flowfield

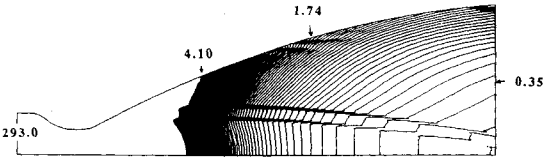

b) Pressure contours of flowfield

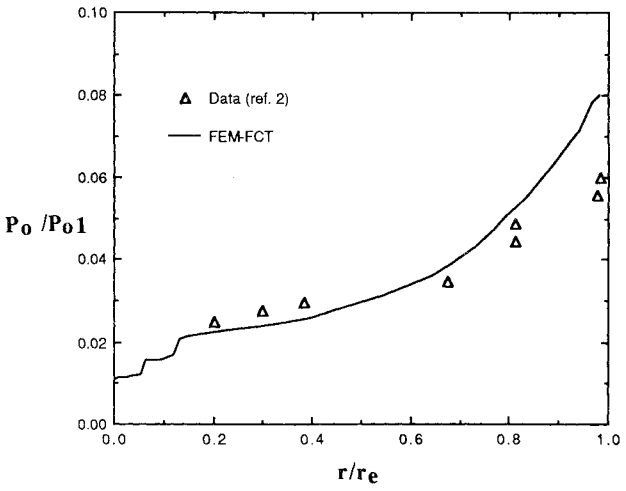

c) Radial distribution of pitot pressure normalized by chamber pressure at the exit plane

Fig. 2 Predictions of a second nozzle flow.

IV. Conclusions

Numerical simulations of axisymmetric supersonic nozzle flow have been accomplished using an axisymmmetric version of the finite element method/flux corrected transport algorithm. The adaptive unstructured gridding and the conservative nonlinear FCT scheme predicted shock formation that agreed with experimental data. Shocks for two given nozzle configurations were observed to form just downstream from the throat due to overexpansion. Axisymmetric effects resulted in increased strength of shocks as they approached the centerline, as well as curvature of compression and expansion waves. The present scheme provided predictions that compared well with experimental results for both radial and axial

flow distributions. This was due to both the high level of cell resolution allowed by the unstructured adaptive mesh and the robust performance of the shock capturing flux limiter.

Acknowledgment

The authors would like to acknowledge valuable discussions with K. Kailasanath, R. Ramamurti, and D. Book.

References

[1]Back, L. H., and Cuffel, R. F., "Detection of Oblique Shocks in a Conical Nozzle with a Circular-Arc Throat," *AIAA Journal,* Vol. 4, No. 12, 1966, pp. 2219-2221.

[2]Thornhill, D., and Ness, R., private communication, Lockheed Missile & Space Co., Palo Alto, CA, 1988-1989.

[3]Adamson, T. C., and Nichols, J. A., "On the Structure of Jets from Highly Underexpanded Nozzles into Still Air," *Journal of Aerospace Sciences,* Vol. 26, No. 1, 1959, pp. 16-24.

[4]Addy, A. L., Dutton, J. C., and Amatucci, V. A., "Nonuniform Nozzle Flow Effects on Base Pressure at Supersonic Flight Speeds," *AIAA Journal,* Vol. 24, No. 7, 1986, pp. 1209-1212.

[5]Serra, J., "Determination of Internal Gas Flows by a Transient Numerical Technique," *AIAA Journal,* Vol. 10, No. 5, 1972, pp. 603-611.

[6]Löhner, R., Baum, J. D., Loth, E., and Ramamurti, R., "A Finite Element Solver for Axisymmetric Compressible Flows," AIAA Paper 89-1794, Buffalo, NY, June, 1989.

[7]Löhner, R., Morgan, K., Peraire, J., and Vahdati, M., "Finite Element Flux Corrected Transport (FEM-FCT) for the Euler and Navier-Stokes Equations," *International Journal of Numerical Methods in Fluids,* Vol. 7, No. 10, 1987, pp. 1093-1109.

[8]Löhner, R., Morgan, K., and Zienkiewicz, O. C., "An Adaptive Finite Element Procedure for High Speed Flows," *Computer Methods in Applied Mechanics and Engineering,* Vol. 51, No. 1-3, 1985, pp. 441-465.

[9]Roe, P. L., "Error Estimates for Cell-Vertex Solvers of the Compressible Euler Equation," Institute for Computer Applications in Science and Engineering, Rept. 87-6, Langley, VA, 1987.

[10]Oran, E. S., and Boris, J. P., *Numerical Simulation of Reactive Flow,* Elsevier, New York, 1987.

[11]Loth, E. Baum, J. D., and Löhner, R., "Formation of Shocks Within Axisymmetric Flows," AIAA Paper 90-1655, Buffalo, NY, June 1990.

Turbulent Boundary-Layer Characteristics over a Flat-Plate/ Wedge Configuration at Mach 6

P. J. Disimile*
University of Cincinnati, Cincinnati, Ohio 45221
and
N. E. Scaggs†
Air Force Wright Research and Development Center, Wright-Patterson Air Force Base, Ohio 45433

Nomenclature

P_0 = stagnation pressure
P_t = local pitot pressure
P_s = static pressure
P_i = surface pressure at a given xy location
P_{ref} = undisturbed reference surface pressure acquired at $x = -6.469$ cm
Re = unit Reynolds number/meter
T_0 = stagnation temperature
T_t = local total temperature
T_s = static temperature
U = local mean velocity
U_{inf} = freestream velocity
x, y, z = streamwise, lateral (along the plate's width), and perpendicular to plate distance
δ = boundary-layer thickness
δ_T = thermal boundary-layer thickness (where T_t is 1% of the freestream)

Presented as Paper 90-3028 at the AIAA 8th Applied Aerodynamics Conference, Portland, OR, Aug. 20-22, 1990; received June 27, 1990; revision received Dec. 28, 1990; accepted for publication Dec. 28, 1990.

*Bradley Jones Associate Professor, Department of Aerospace Engineering. Member AIAA

†Technical Manager. Senior Member AIAA.

Introduction

A RECENT review of aerothermodynamic problems surrounding hypersonic flight and its associated research by Holden[1] demonstrates our present lack of predictive capability. Holden states that the intense research programs of the 1960s and early 1970s were superseded by hypersonic flow investigations that were limited to supporting specific missions such as the Space Shuttle, the Jovian entry vehicle, and ballistic re-entry vehicles. The results of this review vividly point out the scarcity of previous research encompassing turbulent boundary-layer separation and hypersonic flows.

Many earlier studies[2-7] on turbulent boundary-layer separation were preformed on smooth surfaces in supersonic-hypersonic flow regimes. These studies investigated incipient separation using compression corners to simulate flow over aerodynamic flaps or ailerons. Because high-speed flight vehicles employ various external control devices that can produce large areas of flow separation, a program was initiated to examine such effects.

Model and Experimental Facility

A smooth flat-plate/22 deg wedge configuration extending approximately 45.7 cm in streamwise length and 35.6 cm in lateral extent was machined to a no. 32 surface finish. A sharp 10-deg asymmetric leading edge was also machined into the model. Approximately 39.4 cm downstream from this leading edge was the intersection point of the instrumental wedge.

The model was then mounted downstream of a 30.5-cm open jet, high-Reynolds-number, Mach 6 blowdown wind tunnel. By adjusting the total pressure and stagnation temperature, unit Reynolds numbers ranging from approximately 33 to 98 $\times$ 10^6/m were obtained.

Model instrumentation consists of 46 surface pressure points and seven type-K (chromel/alumel) thermocouples. These ports were spaced streamwise in the x direction along the plate at its center ($y = 0$) and ± 9.5 mm off the center through the interaction region.

Boundary-Layer Characteristics

Distribution of both the total pressure and total temperature in the boundary layer were obtained using a pitot pressure probe and a Winkler-type temperature probe. To allow for high-resolution, near-wall total pressure measurements, the tip of the pressure probe was flattened resulting in an overall height of 0.51 mm. For the same reasoning, a miniature Winkler probe was fabricated measuring 1.52 mm in diameter. The recovery factor for this probe was determined to be 0.984 and the uncertainty in the temperature measurement is 2.2 K.

Traverses were performed at two streamwise locations, $x = -16.47$ and -5.52 cm upstream from the plate/wedge intersection point. A third traverse, perpendicular to the ramp surface at a distance along the surface equal to $+3.97$ cm downstream from the intersection point, was also performed. In addition, surface static pressure and wall temperatures were also recorded. From these measurements, the Mach number, velocity, and static temperature through the boundary layer were obtained.[8] Using numerical integration, the momentum thickness θ was computed for each unit Reynolds number and was found to be in good agreement when compared to the em-